

# A single-atom level mechano-optical transducer for ultra-sensitive force sensing

Yang Liu<sup>1,2,\*</sup>, Pengfei Lu<sup>1,\*</sup>, Xinxin Rao<sup>1</sup>, Hao Wu<sup>1</sup>, Kunxu Wang<sup>1</sup>, Qifeng Lao<sup>1</sup>, Ji Bian<sup>1</sup>, Feng Zhu<sup>1,2</sup>, Le Luo<sup>1,2,3</sup>

<sup>1</sup>*School of Physics and Astronomy, Sun Yat-sen University, Zhuhai 519082, China*

<sup>2</sup>*Center of Quantum Information Technology, Shenzhen Research Institute of Sun Yat-sen University, Nanshan Shenzhen 518087, China*

<sup>3</sup>*International Quantum Academy (SIQA), and Shenzhen Branch, Hefei National Laboratory, Futian District, China*

<sup>4\*</sup>*These authors contributed equally to this work*

<sup>5</sup>*E-mail:luole5@mail.sysu.edu.cn*

**Using light as a probe to detect a mechanical motion is one of the most successful experimental approaches in physics. The history of mechanical sensing based on the reflection, refraction and scattering of light dates back to the 16th century, where in the Cavendish experiment, the angle of rotation induced by the gravitational force is measured by the deflection of a light beam reflected from a mirror attached to the suspension. In modern science, mechano-optical transducers are such devices that could detect, measure and convert a force or displacement signal to an optical one, and are widely used for force detection. Especially, ultraweak force sensor with ultrahigh spatial resolution is highly demanded for detecting force anomaly in surface science, biomolecule imaging, and atomtronics. Here we show a novel scheme using a single trapped ion as a mechano-optical transduction. This method utilizes the force-induced micromotion, converting the micromotion to a time-resolved fluorescence signal, in which the ion's excess micromotion coupled to the Doppler shift of the scattered photons. We demonstrate the measurement sensitivity about  $600 \text{ zN}/\sqrt{\text{Hz}}$  ( $1 \text{ zN} = 10^{-21} \text{ N}$ ). By alternating the detection laser beam in all three dimensions, the amplitude and the direction of a vector force can be precisely determined, constituting a 3D force sensor. This mechano-optical transducer provides high sensitivity with spatial resolution in single-atom level, enabling the applications in material industry and the search for possible exotic spin-dependent interactions that beyond the standard model.**

Force sensors with high sensitivity have rich applications in fundamental science and engineering. The ability to measure extremely small forces plays a vital role in absolute gravimetry and inertial navigation <sup>1-3</sup>, determination of gravitational constant  $G$  <sup>4</sup>, gravitational wave detection <sup>5</sup>, force microscopy <sup>6</sup>, and spin-resonance imaging <sup>7</sup> et.al. Dating back in history, since Henry Cavendish's first measurement of the specific gravity of the Earth using torsion balance in 1797, a variety of methods of measuring force have been developed. Among those methods, translating a mechanical signal to an optical signal have been proved to be one of the most sensitive ones, especially recent techniques of using both lasers and quantum sensors for mechano-optical systems, such as micro- and nano-mechanical oscillator <sup>8,9</sup>, optically levitated microspheres <sup>10</sup>, and trapped ions <sup>11</sup>.

All the systems have been applied for sensing very weak electric-magnetic, optical, gravitational and exotic forces. Among these mechano-optical systems, trapped ions enable exquisite control of both spin and motional degrees of freedom<sup>12-15</sup>, and thus allowing quantum-enhanced measurement, therefore it is the most capable platform for detecting ultraweak forces with ultrahigh spatial resolution.

Currently, there are three typical force-sensing scenarios developed with trapped ions. The first one is to image the ion's displacement induced by the force, such as the ultrafast single-photon counting<sup>14</sup> and super-resolution imaging<sup>15,16</sup>. The second one utilizes the Doppler effect, where the force to be measured affects the frequency of the fluorescence photon, including phase-coherent Doppler velocimetry<sup>13</sup>, quantum lock-in detection of the fluorescence<sup>17-19</sup>. The third method employs quantum-enhanced techniques to measure the change of the spin state induced by the force. The experiments along this route include measurements of the Fock states overlaps<sup>20</sup>, amplification of coherent displacements by squeezing<sup>21</sup>, many-body spin echo by entangling the motion mode and the collective spin<sup>18,19</sup>. Based on these techniques, trapped-ion based force sensor has been proposed for various applications. In one hand, it has been suggested for a sensitivity in the yocto-Newton regime, a regime where quantum gravity can be experimentally tested<sup>22,23</sup>. On the other hand, instead of perusing the extreme sensitivity, trapped ions have been proposed for 3D sensing of the force anomaly, where the information of both direction and frequency of the force are lacking before the data acquisition. Therefore, most of the schemes mentioned above are not suitable, since they are designed to measure the forces that are periodically driven.

Here we present a new schemes based on the mechano-optical transduction without requiring modulating the force to be measured, in which the exerted forces acted on a trapped ion can be measured by the fluorescence signal related to the ion's micromotion. With the achieved sensitivity of  $229.17 \text{ zN}/\sqrt{\text{Hz}}$ , our scheme could enable 3D sensing of the force anomaly. It is noted that our method is very different with the force detection using Doppler velocimetry demonstrated in a Penning trap<sup>13</sup>, where the ion's motion is modulated by AC electric force with the axial center-of-mass mode frequency. The method presented in this paper does not require any external modulation of the force. Instead, the force to be measured results in excess micromotion that intrinsically has the same frequency of the driving frequency of the RF field used for trapping, so called the RF-photon correlation<sup>24</sup>. With this technique, by scanning the photon arrival time, phase information of fluorescence is naturally captured, thus providing a lock-in-like measurement of the force. Different with the standard lock-in method, in which the signal to be measured must be modulated and the relative phase between the modulation and demodulation signal are fixed, the RF-photon correlation method can measure a unknown force without modulation. This advantage provide a feasible scheme for sensing of the force anomaly, where the frequency spectrum of the force is usually unknow before the measurement.

*Near-saddle point case.* The initial ion's position is deliberately offset from the saddle point, allowing for the measurement of the force up to a hundred atto-Newtons. We first carried out the force measurement in geometry *I*, where the voltage  $V_3$  on electrode DC3 was varied in small

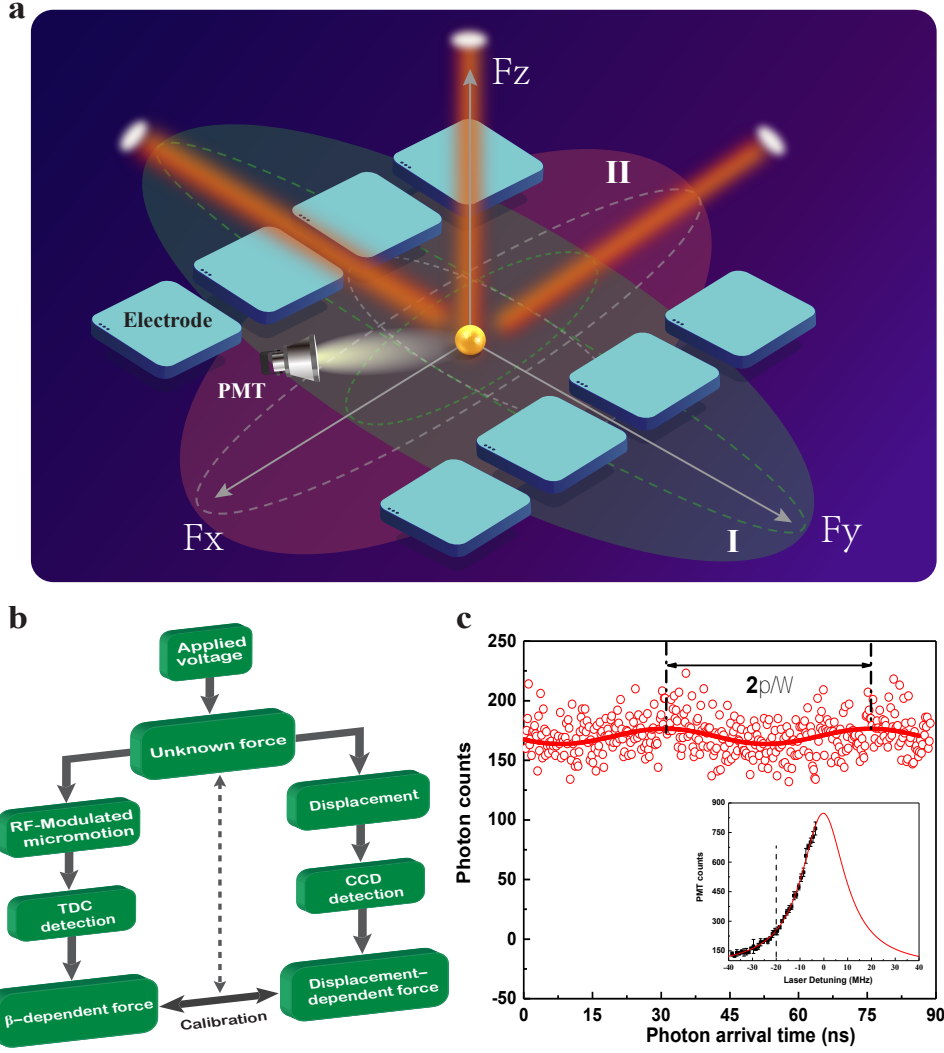


Figure 1: Force sensor based on a trapped ion's excess micromotion. a, The basic schematics of force measurement using mechano-optical transducer. With detection laser along trap axis (or either of the radial principle axis), the force-induced RF-modulated fluorescence is collected by a photomultiplier tube (PMT), by which the three-dimensional geometry of the applied force, e.g. geometry  $I$  (ellipsoid in light green) or  $II$  (ellipsoid in light purple) can be found. b, The experimental flow chart of the force sensing using the mechano-optical transduction scheme. c, The ion's RF-photon correlated fluorescence (red circles), where the histogram of photon arrival times relative to start pulses generated synchronously with the RF driving field is shown. Photon arrivals are bunched with a periodicity dictated by the driven RF frequency. The solid red line is an theoretical fit to the data used to obtain the micromotion index  $\beta$ . The inset shows the resonance profile of the electronic transition  $^2S_{1/2} \leftrightarrow ^2P_{1/2}$ . The black square and red line corresponds to the measurement and theoretical fit. Here, the detuning of the detection laser is chosen as  $\Delta = -2\pi \times 20 \text{ MHz} \approx -\Gamma$  marked by the vertical dashed line, in order to obtain a relatively large photon-correlation signal  $\frac{\Delta}{S_0}$ <sup>25</sup>. The power of the detection laser throughout the experiment is kept in the low intensity limit, i.e. the ion is driven below the saturation limit  $I/I_{sat} \approx 0.5$ .

steps. The micromotion indices, the trapping frequencies, and the ion's images were measured for each  $V_3$ , as shown in Figure 2. In Figure 2(a), we calibrated  $\beta_X$  to the ion's axial displacement  $r_X$  based on the theoretical relation

$$\beta_X = \sqrt{\beta_{X,eff}^2 + \beta_0^2} = \sqrt{(\pi q_X (r_X - r_{X,0})/\lambda)^2 + \beta_0^2}, \quad (1)$$

From this calibration, we determined non-zero  $q_X = 0.00234(5)$  and  $\beta_0 = 0.0318(3)$ , which were attributed to the non-vanishing RF field along the trap axis, and  $r_{X,0} = -1.35(5)\mu m$  was the initial displacement from the RF node. It was evident that all  $\beta_X$  could be well calibrated by  $r_X$  according to Eq. 1. It is noted that contrary to  $q_y$  and  $q_z$ , which can be deduced from the measurements of radial secular frequencies  $\omega_y$  and  $\omega_z$  with varying RF voltages,  $q_X$  cannot be obtained from trap frequency measurements, because the RF potential is never dominant in this direction. By fitting the uncertainties of  $q_X$ ,  $\beta_0$  and  $r_{X,0}$  with this calibration, we estimate that the corrections for the force component  $F_X$  along the axial direction of the linear trap is less than 3.4%. In Figure 2(b), by varying voltage on electrode DC3, the electric forces were attained by following relation modified from Eq.8:

$$F_X = \frac{\lambda m \omega_X^2 \sqrt{\beta_X^2 - \beta_0^2}}{\pi q_X}. \quad (2)$$

Here the trapping frequency  $\omega_X$  was measured independently. As is evident from Figure 2(b), when the applied voltage difference was beyond the range of  $\Delta V_3 = (-0.5V, -0.12V)$ , did  $\beta_X$  and  $F_X$  start to increase monotonically. In the range of  $5 < F_X < 20$  aN, it clearly demonstrated very good linear dependence on the applied voltage.

In Figure 2(c), the calibration of  $\beta_{X,Y}$  to the ion's displacement  $r_X$  and  $r_Y$  is illustrated, which agrees well with the theoretical fit according to

$$\beta_{X,Y} = \sqrt{(\pi q_X (r_X - r_{X,0}) \sin \phi / \lambda + \pi q_{y,z} \cos \phi (r_Y - r_{Y,0}) / \lambda)^2 + \beta_1^2}, \quad (3)$$

whose derivation can be found in Methods Eq.9.  $\phi = 14^\circ$  is the angle between the direction of detection laser and  $Y$  axis in the lab coordinate, which was chosen for the minimization of the background scattering from the vacuum viewport windows.  $q_{y,z} = \sqrt{q_y q_z} = 0.209$ .  $r_{Y,0} = -0.03(4)\mu m$  is the initial displacement from the RF node.  $\beta_1 = 0.077(19)$  originates from both the non-vanishing RF field along the trap axis and the residual phase shifts of the RF potential on the opposing radial electrodes. Thus, based on the measurement of the micromotion indices and the ion's position displacements, the electric forces were attained by

$$\begin{aligned} F_{X,Y} &= m \omega_Y^2 (r_Y - r_{Y,0}) \\ &= \frac{\lambda m \omega_Y^2 \sqrt{\beta_{X,Y}^2 - \beta_1^2} - \sqrt{\beta_X^2 - \beta_0^2} \sin \phi}{\pi q_{y,z} \cos \phi}, \end{aligned} \quad (4)$$

where  $\omega_Y = \sqrt{\omega_y^2 \cos^2 \theta + \omega_z^2 \sin^2 \theta}$  is the oscillation frequency along the  $Y$  axis, as shown in Figure 2(d). Compared to the axial force  $F_X$ , the radial force  $F_{X,Y}$  is more sensitive and illustrates

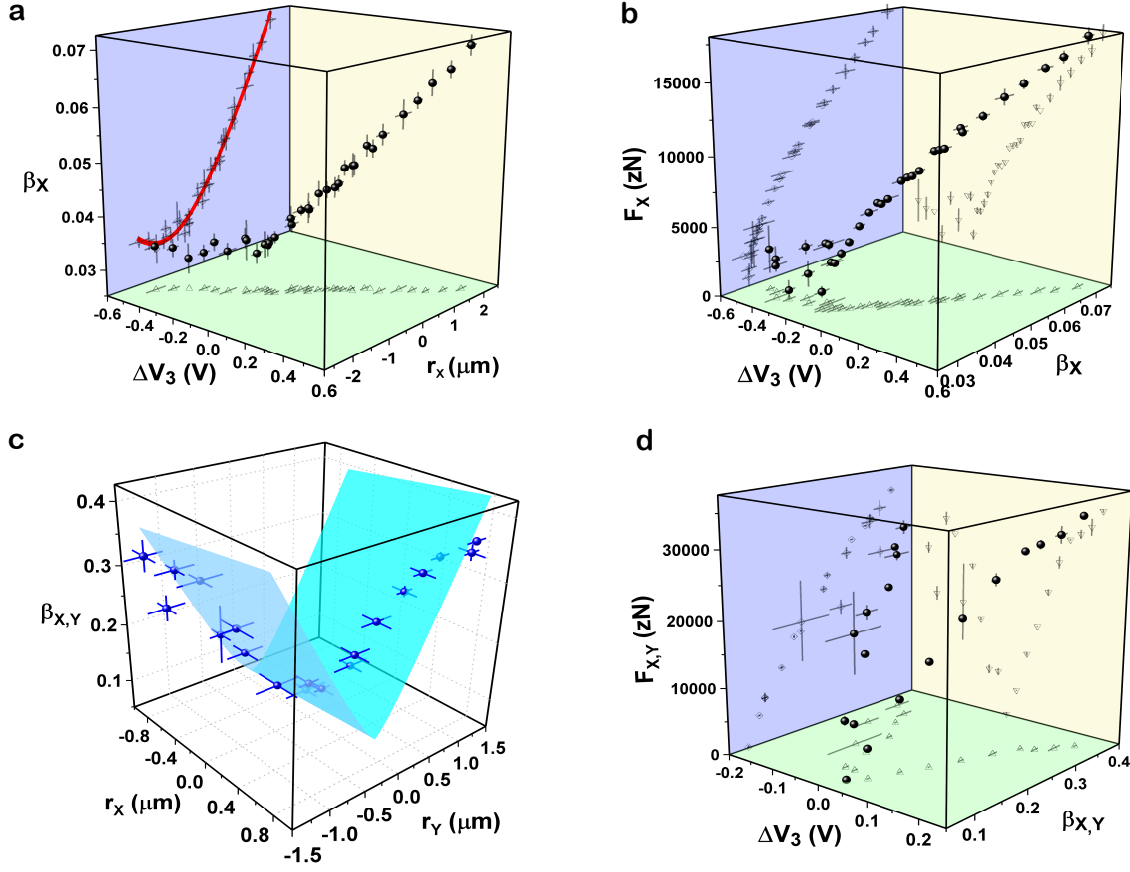


Figure 2: The measurements of electric forces in geometry *I*. (a) The calibration of  $\beta_X$  to the ion's axial displacement  $r_X$  at various  $\Delta V_3$ . The black spheres with error bars are experimental data from independent RF-photon correlation measurements and imaging measurements, while triangles (diamonds) are projections to the  $\Delta V_3 - r_X$  ( $r_X - \beta_X$ ) plane, representing the dependence of the ion's axial displacement on the applied voltage (the correspondence of the micromotion index in trap axis to the ion's axial displacement). The red line on the  $r_X - \beta_X$  plane is the theoretical fit to Eq.1. (b) The dependence of axial electric force  $F_X$  on the applied voltage and micromotion index  $\beta_X$ . The triangles, inverted triangles and diamonds represent the dependence of the micromotion index  $\beta_X$  on the applied voltage, axial force  $F_X$  on the applied voltage and on the micromotion index  $\beta_X$ , respectively. (c) The calibration of  $\beta_{X,Y}$  to the ion's displacement  $r_X$  and  $r_Y$  at various applied voltages. The blue spheres with error bars are experimental data, and the cyan surface is the theoretical fit to Eq.3. (d) The dependence of electric force  $F_{X,Y}$  on the applied voltage and micromotion index  $\beta_{X,Y}$ . The triangles, inverted triangles and diamonds represent the dependence of the micromotion index  $\beta_{X,Y}$  on the applied voltage, force  $F_{X,Y}$  on the applied voltage and on the micromotion index  $\beta_{X,Y}$ , respectively.

a nearly symmetric dependence on  $\Delta V_3$  as what we expected, despite of relatively large systematic uncertainty. The minimal detected force is  $F_X = 653.98 \pm 743.16$  zN and  $F_{X,Y} = 119.69 \pm 331.91$  zN in 30 s measurement time, corresponding to a measurement sensitivity about  $3582.00$  zN/ $\sqrt{\text{Hz}}$  and  $655.57$  zN/ $\sqrt{\text{Hz}}$ , respectively <sup>27</sup>.

The forces in geometry *II*, generated by varying the voltage on a pair of axial-symmetric electrodes DC2 and DC7, were also measured. Figure 3 shows the dependence of the axial force  $F_X$  and the radial force  $F_{X,Y}$  on  $\Delta V_{2,7}$ . In Figure 3(a),  $F_X$  varies nearly symmetric with  $\Delta V_{2,7}$ .  $F_{X,Y}$  is more sensitive to  $\Delta V_{2,7}$  compared with  $F_X$ . The minimal detected force is  $F_X = 951.13 \pm 3030.95$  zN and  $F_{X,Y} = 329.39 \pm 295.42$  zN in 30 s measurement time, corresponding to a measurement sensitivity about  $5209.55$  zN/ $\sqrt{\text{Hz}}$  and  $1804.14$  zN/ $\sqrt{\text{Hz}}$ , respectively.

*At saddle point case.* We performed the force measurements exactly at the saddle point. In order to investigate the best force sensitivity, the ion is close to the saddle point as possible as we could by by the applying machine learning approach <sup>26</sup>. By applying voltages on DC2 and DC7, we obtain a linear dependence of  $\beta_X$  on the applied voltage  $V_2$  and  $V_7$ , shown in Figure 4, while  $\beta_Y \approx 0$  for all the voltage sets, indicating that the ion moves along the trap axis  $X$ . The applied force is then deduced according to Eq. 2. The inset in Figure 4 shows the histogram measured at  $V_2 = 11.75$  V (red circles) and  $V_2 = 12.25$  V (blue triangles) as well as their theoretical fits (solid lines). The corresponding micromotion index are  $\beta_X = 0.0030$  and  $\beta_X = 0.0306$ . The minimal detected force is  $F_X = 514.37 \pm 560.78$  zN in 30 s measurement time, corresponding to a measurement sensitivity about  $2817.32$  zN/ $\sqrt{\text{Hz}}$ , which is about 2 fold better than near saddle-point case.

We have demonstrated a proof-of-principle experiment for measuring extremely weak electric forces using a mechano-optical transducer with a single trapped ion. Comparing with other sensing techniques with trapped ions, our method of mechano-optical transduction can measure a unknown force without having the knowledge of their frequency spectrum, thus distinguishing itself for 3D sensing of force anomaly. For this application, electric forces in two different geometries have been accurately measured by alternating the detection laser between  $X$  and  $Y$  axes, illustrating an excellent 3D force sensor given full optical access in three dimensions. Furthermore, electric forces down to  $F_X = 514.37 \pm 560.78$ zN and  $F_{X,Y} = 119.69 \pm 331.91$ zN have been acquired in 30 s data acquisition time with a sensitivity of  $2817.32$  zN/ $\sqrt{\text{Hz}}$  and  $655.57$ zN/ $\sqrt{\text{Hz}}$  in  $X$  and  $Y$  axis, respectively. The experimental uncertainty includes statistical fluctuations in averaging over the ion fluorescence, the uncertainty in the fitted micromotion index, the uncertainty in the calibration of the applied electric field due to relatively large coma aberrations in the ion image, the uncertainty in the measured trapping frequencies, and the uncertainty in the trap stability q-parameter.

Further improvements are possible for a better sensitivity. First, detection efficiency can be enhanced by realistic modifications and update of current experimental setup, for instance, larger solid angle for fluorescence light collection enabled by a binary phase Fresnel lens with  $NA = 0.64$  <sup>15</sup> or by integration with a glass vacuum cell <sup>28</sup>, using a superconducting single photon de-

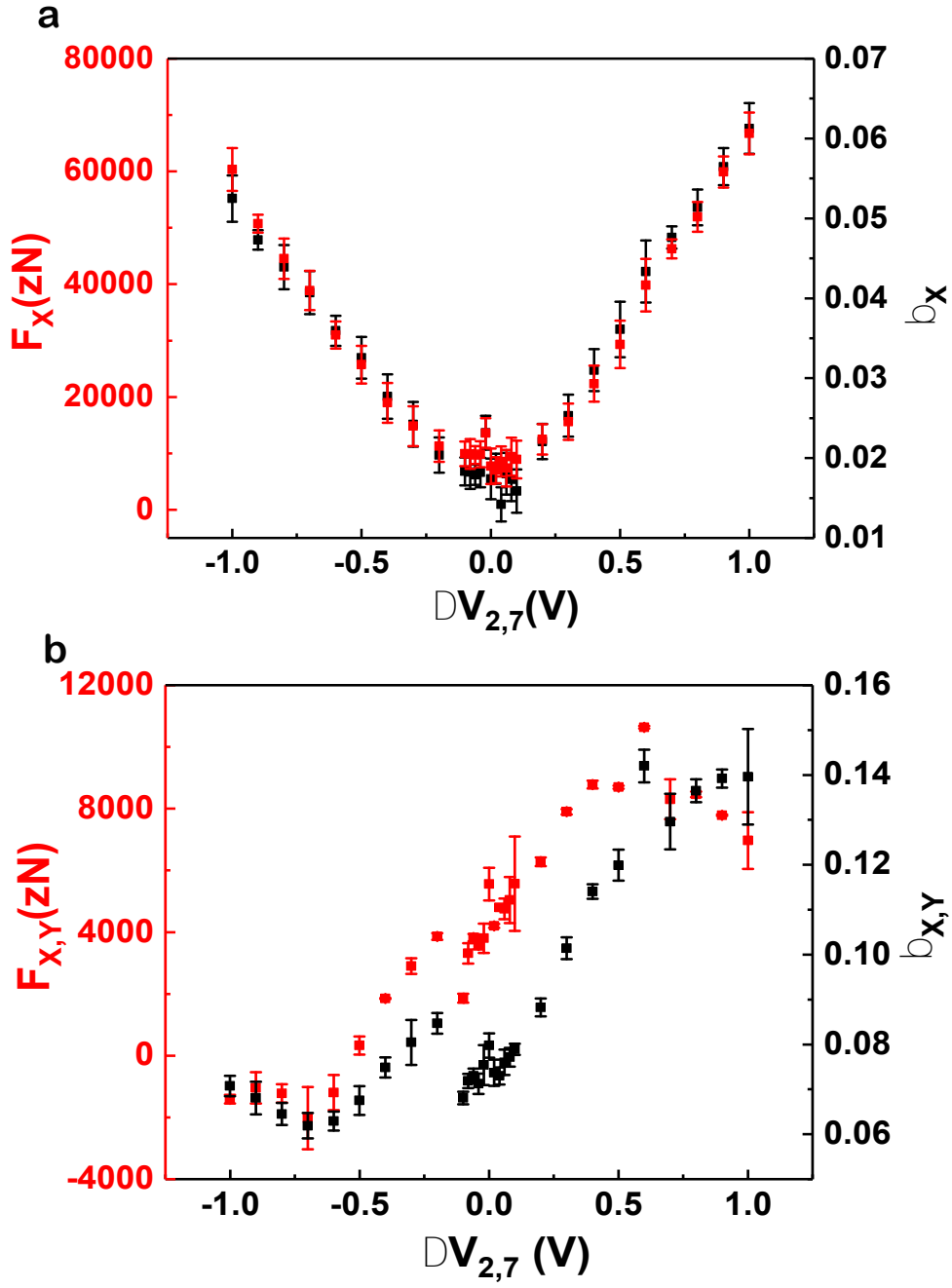


Figure 3: The measurements of electric forces in geometry *II*. (a) The dependence of the micromotion index  $\beta_X$  and force component  $F_X$  on the  $\Delta V_{2,7}$ . (b) The dependence of the micromotion index  $\beta_{X,Y}$  and force component  $F_{X,Y}$  on the  $\Delta V_{2,7}$ .

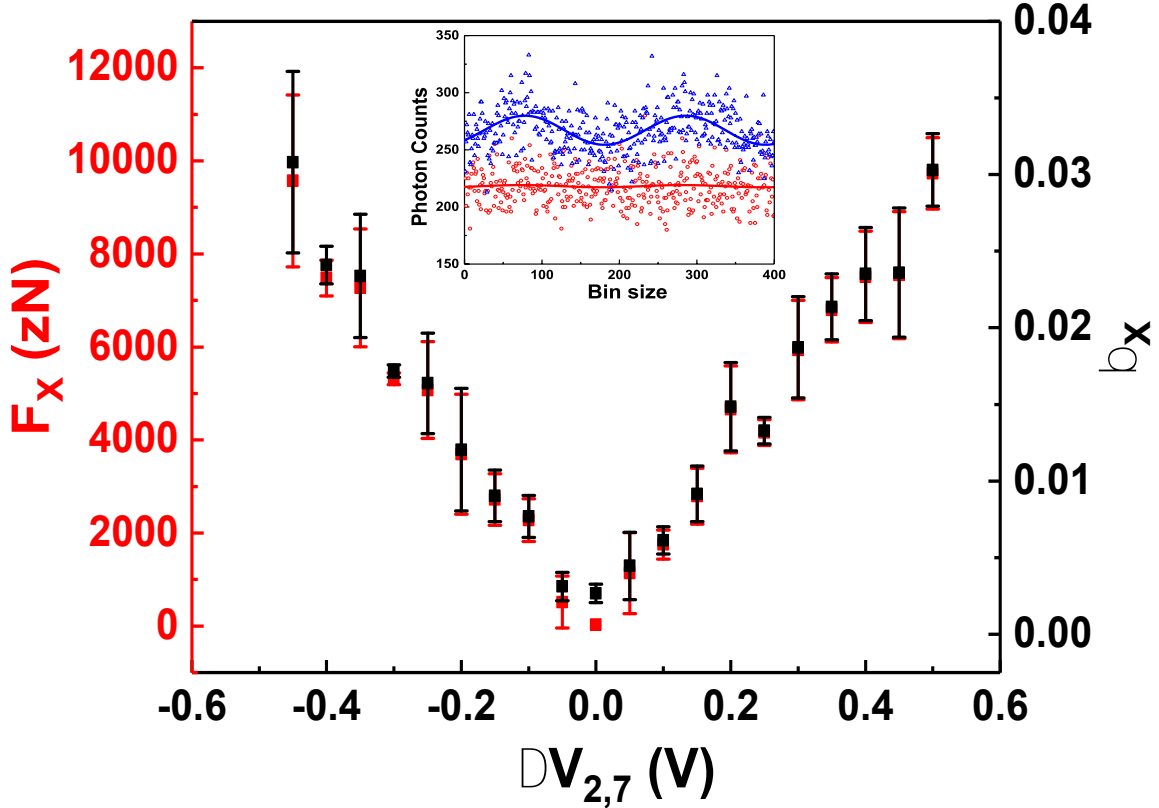


Figure 4: Electric force Detection at the saddle point. The dependence of  $\beta_x$  on  $\Delta V_{2,7}$ . The micromotion is minimized at the saddle point with the micromotion indices of  $\beta_X = 0.0027(6)$  and  $\beta_Y = 0.0308(28)$ , and  $q_y = 0.1827$  and  $q_z = 0.1840$  obtained from the trapping frequency dependence on the applied RF voltage.  $V_2$  and  $V_7$  were varied simultaneously in small voltage step  $\Delta V = 50$  mV, and their relation was  $V_7 = V_2 + 0.25V$ . In the inset, the red circle (blue triangle) and solid line correspond to the histogram measured at  $V_2 = 11.75V$  ( $V_2 = 12.25V$ ) and its fitting, respectively. The corresponding micromotion index is  $\beta_X = 0.0030$  ( $\beta_X = 0.0306$ ).



tectors with  $\approx 80\%$  detection efficiency<sup>29,30</sup> compared to current photon multiplier tube with a nominal 32% at 370 nm. Adapting both improvements would result in a factor of  $\times 4$  enhancement in detection efficiency, providing up to 2-fold increase in the force detection sensitivity. According to Eq. 8 and the pseudopotential approximation<sup>31</sup>,

$$F_i \approx \frac{\lambda m \beta_i \Omega^2}{4\pi} \left( \frac{a_i}{q_i} + \frac{q_i}{2} \right) \geq \frac{\lambda m q_i \beta_i \Omega^2}{4\pi}, \quad (5)$$

where  $\Omega$  is the RF driving frequency. The minimal detectable electric force can be achieved for  $q_i = \sqrt{2a_i}$ . Therefore, additional optimization of the trapped-ion setup, such as trapping a different species with smaller mass and reducing the driving RF frequency could allow us to further enhance the sensitivity by more than four orders of magnitude. As an example, with single trapped  ${}^9\text{Be}^+$ <sup>32</sup>, the RF frequency  $\Omega = 2\pi \times 1.4$  MHz,  $q_i = 0.017$ ,  $\beta_i = 0.001$  for a segmented linear RF trap<sup>33</sup>, it is possible to discriminate electric force of well below 1 yN ( $1 \text{ yN} = 10^{-24} \text{ N}$ ) with a sensitivity  $\approx 2 \text{ yN}/\sqrt{\text{Hz}}$ . Such a single-atom level mechano-optical transducer would provide opportunities to search for the fifth-force beyond the standard model<sup>34</sup>, including exotic spin-dependent force<sup>35–40</sup> and other types of the new forces<sup>41,42</sup>.

**Acknowledgements** This work is supported by the Key-Area Research and Development Program of Guang Dong Province under Grant No.2019B030330001, the National Natural Science Foundation of China under Grant No.11774436, No.11974434 and No. 12074439. Le Luo received supports from Guangdong Province Youth Talent Program under Grant No.2017GC010656, Sun Yat-sen University Core Technology Development Fund. Yang Liu acknowledges the support from Natural Science Foundation of Guangdong Province under Grant 2020A1515011159, and Science and Technology Program of Guangzhou, China 202102080380.

1. Niebauer, T., Sasagawa, G., Faller, J. E., Hilt, R. & Klocking, F. A new generation of absolute gravimeters. *Metrologia* **32**, 159 (1995).
2. Bidel, Y. *et al.* Compact cold atom gravimeter for field applications. *Applied Physics Letters* **102**, 144107 (2013).
3. Battelier, B. *et al.* Development of compact cold-atom sensors for inertial navigation. In *Quantum Optics*, vol. 9900, 990004 (International Society for Optics and Photonics, 2016).
4. Cavendish, H. Xxi. experiments to determine the density of the earth. *Philosophical Transactions of the Royal Society of London* 469–526 (1798).
5. Abbott, B. P. *et al.* Gw170817: observation of gravitational waves from a binary neutron star inspiral. *Physical Review Letters* **119**, 161101 (2017).
6. Binnig, G., Quate, C. F. & Gerber, C. Atomic force microscope. *Physical review letters* **56**, 930 (1986).

7. Rugar, D., Budakian, R., Mamin, H. & Chui, B. Single spin detection by magnetic resonance force microscopy. *Nature* **430**, 329–332 (2004).
8. Stowe, T. *et al.* Attonewton force detection using ultrathin silicon cantilevers. *Applied Physics Letters* **71**, 288–290 (1997).
9. Mamin, H. & Rugar, D. Sub-attonewton force detection at millikelvin temperatures. *Applied Physics Letters* **79**, 3358–3360 (2001).
10. Geraci, A. A., Papp, S. B. & Kitching, J. Short-range force detection using optically cooled levitated microspheres. *Physical review letters* **105**, 101101 (2010).
11. Blatt, R. & Wineland, D. Entangled states of trapped atomic ions. *Nature* **453**, 1008–1015 (2008).
12. Maiwald, R. *et al.* Stylus ion trap for enhanced access and sensing. *Nature Physics* **5**, 551–554 (2009).
13. Biercuk, M. J., Uys, H., Britton, J. W., VanDevender, A. P. & Bollinger, J. J. Ultrasensitive detection of force and displacement using trapped ions. *Nature nanotechnology* **5**, 646–650 (2010).
14. Knünz, S. *et al.* Injection locking of a trapped-ion phonon laser. *Physical review letters* **105**, 013004 (2010).
15. Blüms, V. *et al.* A single-atom 3d sub-attonewton force sensor. *Science advances* **4**, eaao4453 (2018).
16. Wong-Campos, J., Johnson, K., Neyenhuis, B., Mizrahi, J. & Monroe, C. High-resolution adaptive imaging of a single atom. *Nature Photonics* **10**, 606–610 (2016).
17. Shaniv, R. & Ozeri, R. Quantum lock-in force sensing using optical clock doppler velocimetry. *Nature communications* **8**, 1–5 (2017).
18. Gilmore, K. A., Bohnet, J. G., Sawyer, B. C., Britton, J. W. & Bollinger, J. J. Amplitude sensing below the zero-point fluctuations with a two-dimensional trapped-ion mechanical oscillator. *Physical review letters* **118**, 263602 (2017).
19. Gilmore, K. A. *et al.* Quantum-enhanced sensing of displacements and electric fields with two-dimensional trapped-ion crystals. *Science* **373**, 673–678 (2021).
20. Wolf, F. *et al.* Motional fock states for quantum-enhanced amplitude and phase measurements with trapped ions. *Nature communications* **10**, 1–8 (2019).
21. Burd, S. *et al.* Quantum amplification of mechanical oscillator motion. *Science* **364**, 1163–1165 (2019).

22. Kafri, D., Taylor, J. & Milburn, G. A classical channel model for gravitational decoherence. *New Journal of Physics* **16**, 065020 (2014).
23. Albrecht, A., Retzker, A. & Plenio, M. B. Testing quantum gravity by nanodiamond interferometry with nitrogen-vacancy centers. *Physical Review A* **90**, 033834 (2014).
24. Berkeland, D., Miller, J., Bergquist, J. C., Itano, W. M. & Wineland, D. J. Minimization of ion micromotion in a paul trap. *Journal of applied physics* **83**, 5025–5033 (1998).
25. Keller, J., Partner, H., Burgermeister, T. & Mehlstäubler, T. Precise determination of micromotion for trapped-ion optical clocks. *Journal of Applied Physics* **118**, 104501 (2015).
26. Liu, Y. *et al.* Minimization of the micromotion of trapped ions with artificial neural networks. *Applied Physics Letters* **119**, 134002 (2021).
27. Degen, C. L., Reinhard, F. & Cappellaro, P. Quantum sensing. *Reviews of modern physics* **89**, 035002 (2017).
28. He, R. *et al.* An ion trap apparatus with high optical access in multiple directions. *Review of Scientific Instruments* **92**, 073201 (2021).
29. Crain, S. *et al.* High-speed low-crosstalk detection of a 171 yb+ qubit using superconducting nanowire single photon detectors. *Communications Physics* **2**, 1–6 (2019).
30. Todaro, S. L. *et al.* State readout of a trapped ion qubit using a trap-integrated superconducting photon detector. *Physical Review Letters* **126**, 010501 (2021).
31. Paul, W. Electromagnetic traps for charged and neutral particles. *Reviews of modern physics* **62**, 531 (1990).
32. Meekhof, D., Monroe, C., King, B., Itano, W. & Wineland, D. Generation of nonclassical motional states of a trapped atom [phys. rev. lett. 76, 1796 (1996)]. *Physical Review Letters* **77**, 2346 (1996).
33. Schmidt, J. *et al.* Mass-selective removal of ions from paul traps using parametric excitation. *Applied Physics B* **126**, 1–7 (2020).
34. Safronova, M. *et al.* Search for new physics with atoms and molecules. *Reviews of Modern Physics* **90**, 025008 (2018).
35. Dobrescu, B. A. & Mocioiu, I. Spin-dependent macroscopic forces from new particle exchange. *Journal of High Energy Physics* **2006**, 005 (2006).
36. Kotler, S., Akerman, N., Navon, N., Glickman, Y. & Ozeri, R. Measurement of the magnetic interaction between two bound electrons of two separate ions. *Nature* **510**, 376–380 (2014).
37. Kotler, S., Ozeri, R. & Kimball, D. F. J. Constraints on exotic dipole-dipole couplings between electrons at the micrometer scale. *Physical review letters* **115**, 081801 (2015).

38. Chen, Y.-J. *et al.* Stronger limits on hypothetical yukawa interactions in the 30–8000 nm range. *Physical review letters* **116**, 221102 (2016).
39. Rong, X. *et al.* Searching for an exotic spin-dependent interaction with a single electron-spin quantum sensor. *Nature communications* **9**, 1–7 (2018).
40. Almasi, A., Lee, J., Winarto, H., Smiciklas, M. & Romalis, M. V. New limits on anomalous spin-spin interactions. *Physical review letters* **125**, 201802 (2020).
41. Ding, J. *et al.* Constraints on the velocity and spin dependent exotic interaction at the micrometer range. *Physical review letters* **124**, 161801 (2020).
42. Jiao, M., Guo, M., Rong, X., Cai, Y.-F. & Du, J. Experimental constraint on an exotic parity-odd spin-and velocity-dependent interaction with a single electron spin quantum sensor. *Physical Review Letters* **127**, 010501 (2021).

**Methods** In a typical Paul trap, when the ion is disturbed by an additional static electric field  $E_{dc}$ , its equation of motion can be written as <sup>24</sup>:

$$\ddot{u}_i + [a_i + 2q_i \cos(\Omega t)] \frac{\Omega^2}{4} u_i = \frac{qE_i}{m}. \quad (6)$$

For  $|q_i| \ll 1$  and  $|a_i| \ll 1$ , the solution to lowest order in  $q_i$  and  $a_i$  is

$$u_i(t) \cong [r_i + s_i \cos(\omega_i t + \phi_{si})] [1 + \frac{q_i}{2} \cos(\Omega t + \phi_i)], \quad (7)$$

where  $r_i \cong \frac{4eE_i}{m(a_i + \frac{q_i^2}{2})\Omega^2} \cong \frac{eE_i}{m\omega_i^2}$  is a displacement of the equilibrium position from the rf node for a trapped ion with charge  $e$  and mass  $m$ .  $s_i$  is the secular motion amplitude with the frequency of  $\omega_i = \frac{\Omega}{2} \sqrt{a_i + \frac{q_i^2}{2}}$ .  $\phi_{si}$  is the phase of secular motion determined by the initial conditions of the ion position and velocity.  $\phi_i$  is the phase of the micromotion.

This solution describes that for a trapped ion near the saddle point of the RF trapping potential, a weak electric force  $q\vec{E}_i$  would not only shift the ion's equilibrium position by  $r_i$ , but also induces an excess micromotion modulated by the RF frequency of  $\Omega$  with an amplitude of  $\frac{1}{2}r_i q_i$  along  $\hat{u}_i$  at position  $r_i$ . With the assumption of zero phase difference between two ac electrodes  $\phi_{ac} = 0$ , the micromotion index is described by  $\beta_i = \frac{1}{2}k_i q_i |r_i|$ , where  $k_i$  is the component of wave vector on axis  $i$ . Since  $q_i$  is proportional  $V_{RF}/\Omega^2$  and is dependent on the trap's geometric configuration, it would not change by varying the DC voltages, therefore the micromotion index is proportional to the ion's displacement  $\beta_i \propto r_i$ . Because of the coefficient  $kq_i/2 = \pi q_i/\lambda \gg 1$  for a typical Paul trap (in our case,  $q_x \sim 4 \times 10^{-4}$  and  $q_{y,z} \sim 0.2$ ) and ultraviolet (or visible) lasers, it would bring a large amplification effect on measuring a weak force. Thus, an extremely weak electric force which cannot be detected by displacement measurement from imaging method, can be precisely measured through measurement of  $\beta_i$  using RF-photon correlation technique <sup>25</sup>.

In our experiment, weak unknown force is generated by applying a small electric DC voltage to the DC electrodes of the trap. Then the excess micromotion generates a fluorescence signal modulated by the RF frequency. The fluorescence is detected by the photomultiplier tube (PMT) and is successively analyzed by the time-to-digital converter (TDC). The experimental schematics, detailed experimental sequences and demodulated ion's fluorescence are shown in Figure 1. The micromotion index  $\beta_i$  is inferred by fitting the recorded fluorescence histogram to the model of damped harmonic oscillator <sup>25,26</sup>. The force related to the micromotion is determined by

$$F_i = \frac{\lambda m \omega_i^2 \beta_i}{\pi q_i} \propto \Delta V, \quad (8)$$

since  $\beta_i = \frac{1}{2}k_i q_i r_i = \pi q_i e E_i / \lambda m \omega_i^2$ . Therefore, a three-dimensional force can be precisely determined from micromotion indices, which can be measured simply by alternating the detection laser between three axes, i.e. the three principal axes of the trap. Such a method have a intrinsical lock-in function, where the modulated and demodulated signal are mechanical and optical, respectively.

Consequently, this system constitutes a mechano-optical transducer at a single atom level. Such a transducer not only has extremely high spatial resolution, but also has the advantages over standard lock-in technique, because it continuously scans the phase between modulated and demodulated signal, thus enabling the detection of force of unknown frequency spectrum. For developing a force sensor, there usually has to be a compromise between detection sensitivity and measurement range. In our system, the best force sensitivity can be achieved when the ion's unperturbed position exactly at the saddle point, while the larger force range can be obtained when the ion's unperturbed position have a limited offset to the saddle point.

In this method, since the fluorescence is modulated by the RF frequency and its second harmonics<sup>24,25</sup>, any noise which is hardly in phase with the RF frequency, and averaging over  $N \gg 1$  times, would greatly enhance the contrast of the desired signal relative to the background noise by a factor of  $N^{1/2}$ , similar to the phase-coherent Doppler velocimetry<sup>13</sup>.

Practically, in order to realize 3D force sensing, the force measurement were carried out in two different force geometries by varying the voltages of the different DC electrodes. In the force detection for both geometries, the axial and radial forces were measured by alternately switching the detection laser between axis  $X$  (the trap axis) and  $Y$  in lab coordinate. In geometry  $I$ , the forces are applied by only varying the voltage on electrode DC3, while in geometry  $II$ , the forces are applied by only varying the voltage on electrodes DC2 and DC7. The ion's displacements are also measured by recording the ion's images at various voltage  $V_i$  for calibration purposes. From these measurements, the dependence of the  $\beta_i$  on the applied voltage  $V_i$ , as well as the dependence of the ion's displacement  $r_i$  on  $V_i$ , which provides a direct calibration of the relation between the micromotion index  $\beta_i$  and the ion's displacement  $r_i$  using two independent methods, are obtained.

The calibration of  $\beta_{X,Y}$  to the ion's displacement  $r_X$  and  $r_Y$  is given by

$$\begin{aligned}
\beta_{X,Y} &= \sqrt{(\beta_{X,eff} \sin \phi + \beta_{y,eff} \cos \phi \cos \theta + \beta_{z,eff} \cos \phi \sin \theta)^2 + \beta_1^2} \\
&= \sqrt{\left(\frac{\pi q_X (r_X - r_{X,0}) \sin \phi / \lambda + \pi q_y (r_y - r_{y,0}) \cos \phi \cos \theta / \lambda}{+ \pi q_z (r_z - r_{z,0}) \cos \phi \sin \theta / \lambda}\right)^2 + \beta_1^2} \\
&\simeq \sqrt{\left(\frac{\pi q_X (r_X - r_{X,0}) \sin \phi / \lambda + \pi q_{y,z} \cos \phi [(r_y - r_{y,0}) \cos \theta}{+(r_z - r_{z,0}) \sin \theta] / \lambda}\right)^2 + \beta_1^2} \\
&= \sqrt{(\pi q_X (r_X - r_{X,0}) \sin \phi / \lambda + \pi q_{y,z} \cos \phi (r_Y - r_{Y,0}) / \lambda)^2 + \beta_1^2}
\end{aligned} \tag{9}$$

where  $\theta \approx 53^\circ$  is the angle between  $Y$  axis and principal axis  $y$  in the radial plane. Its variation with the applied voltage was much smaller than one degree and thus was ignored in this analysis.  $r_{y,0}$  and  $r_{z,0}$  is the initial displacement in principal axes  $y$  and  $z$ , respectively.  $q_y$  and  $q_z$  are linearly proportional to the RF voltage theoretically, and  $q_y \approx 0.203(2)$  and  $q_z \approx 0.215(3)$  were obtained from measurements of radial trapping frequency as a function of RF voltage.

**Experimental Setup** Our force detection is performed on a single  $^{171}\text{Yb}^+$  ion confined in a linear Paul trap similar to Ref [26]. It consists of four gold-plated ceramic blade electrodes, where two opposite blades labelled as RF1 and RF2 are driven with an RF potential, creating the transverse (y-z) quadrupole confinement potential and other two opposite blades each have five segments serving to confine the ion along the x-axis. The RF voltages are fed through a pair of home-made helical resonator (quality factor  $Q \approx 300$ ) and a directional coupler (Mini Circuits ZEDC-15-2B) and a RF amplifier (Mini Circuits LZY-22+) to the RF source (Rigol DSG821). Each electrode is connected to a programmable precision DC voltage power supply (BS1-16-14, Stahl-electronics). The gap between the electrodes is  $470 \mu\text{m}$  and  $220 \mu\text{m}$  in Y and Z direction, respectively. The distance from the trap center to the electrodes  $R \approx 259 \mu\text{m}$ . The cooling laser is  $369.5 \text{ nm}$  from a frequency-doubled Ti: Sapphire laser (M Squared Lasers Ltd, ECD-F) with its fundamental frequency is stabilized using acousto-optic modulation transfer spectroscopy of Iodine, and the repumping lasers are  $935 \text{ nm}$  and  $638 \text{ nm}$  lasers (Toptica, DLC DL PRO).

The ion images in x-y lab coordinate plane are recorded with an electron-magnified charge-coupled device (Andor, ixon-ultra-897 EMCCD). In our imaging optics, the isotropic fluorescence from the ion at  $\lambda=369.5 \text{ nm}$  is transmitted through a vacuum viewport and collected by an objective lens of numerical aperture  $\text{NA} = 0.397$  with  $\times 10$  magnification. The intermediate image passes through a pinhole for spatial filtering and subsequently magnified by another lens with  $\times 50$  magnification in total.

The ion fluorescence passes the same imaging ion optics, and the temporal profile of ion fluorescence due to the applied drive is detected by recording scattered-photon arrival times using a photomultiplier tube (H10682-210, Hamamatsu) relative to a homemade edge-triggered D-type flip-flop electronics. Photon arrival times are then determined over  $N$  iterations of the experiment through demodulation using a START-STOP time-to-digital converter (HRM-TDC, SensL).

For the force detection near saddle-point, the initial voltages on electrodes DC1, DC2,  $\dots$  DC12 were  $9.69 \text{ V}$ ,  $9.88 \text{ V}$ ,  $1.867 \text{ V}$ ,  $10.05 \text{ V}$ ,  $10.05 \text{ V}$ ,  $9.69 \text{ V}$ ,  $9.88 \text{ V}$ ,  $2.0 \text{ V}$ ,  $10.05 \text{ V}$ ,  $10.05 \text{ V}$ ,  $0.186 \text{ V}$  and  $0.01 \text{ V}$ , respectively. The amplitude of RF voltage was  $206.48 \text{ V}$  with the frequency of  $2\pi \times 21.250 \text{ MHz}$ . The corresponding trapping frequencies were  $\omega_x \sim 2\pi \times 721.66 \text{ kHz}$ ,  $\omega_y \sim 2\pi \times 1.184 \text{ MHz}$  and  $\omega_z \sim 2\pi \times 1.602 \text{ MHz}$ , respectively.

While for the force detection at saddle-point, the applied voltages were  $(V_1, V_2 \dots V_{12}, V_{RF}) = (11.75 \text{ V}, 11.75 \text{ V}, 1.754 \text{ V}, 9.35 \text{ V}, 9.35 \text{ V}, 12 \text{ V}, 12 \text{ V}, 1.9 \text{ V}, 9.6 \text{ V}, 9.6 \text{ V}, -0.079 \text{ V}, -0.22 \text{ V}, 227.84 \text{ V})$  at  $0.45 \text{ W}$  RF power and  $\Omega = 2\pi \times 22.625 \text{ MHz}$  RF frequency. The corresponding trapping frequencies were  $(\omega_x, \omega_y, \omega_z) = (2\pi \times 0.748, 2\pi \times 1.382, 2\pi \times 1.655) \text{ MHz}$ .